Study on Fast Fracture and Crack Arrest

Experimental results of brittle-crack propagation and arrest on structural steel are analyzed using the finite-difference method

by T. Kanazawa, S. Machida, T. Teramoto and H. Yoshinari

ABSTRACT—In this paper, the experimental results of brittle-crack propagation and arrest on structural steels are analyzed using the finite-difference method. The test specimens used are double-tension and double-cantilever type (DCB).

It is found that dynamic consideration is indispensable for general interpretation of fast fracture and crack arrest and material toughness can be defined as a function of temperature and crack velocity. Using the defined fracture toughness, crack-propagation-arrest behavior can be predicted by crack-propagation simulation if the condition of boundary loading of a specimen is known. This implies a possibility to develop simple methods for crack-arrester design.

Introduction

Since the shipbuilding industries experienced a number of catastrophic failures due to brittle fracture, naval architects have been interested in the brittle fracture of ship structural steels. Japanese research groups conducted extensive series of brittle-crack propagation and arrest experiments in low and medium strength steels using wide-plate tension specimens including very wide (about 2.5-m) specimens, and tried to apply fracture mechanics to interpret the results of brittle-fracture-propagation arrest tests and to define material toughness against a rapidly propagating crack.

For a rapidly propagating crack which propagates only a short distance, static analysis based on linear-fracture mechanics at the instant of crack arrest can be used to estimate a crack-arrest fracture toughness. For a crack propagating over a longer distance observed in very wide plate experiments, however, static approximation fails to correlate the various experimental data on crack arrest.[1]

It is considered that the experimentally proven inadequacy of crack-arrest theory based on simple static analysis may be attributable to the fact that dynamic aspects associated with fast crack propagation have been disregarded. Thus, the dynamic behavior of fast fracture and crack arrest is a matter of renewed concern today to structural engineering. In search of a more relevant theoretical basis for crack-arrest methodology in design, the authors have been conducting various brittle-crack propagation and arrest experiments in ship-hull steels and attempted to interpret the experimental data on a fracture-dynamic basis.

Unfortunately, the dynamic fracture toughness during and at arrest of a rapidly propagating crack in steel plate cannot be measured directly and thus must be deduced by an indirect procedure. The method used in this paper is to use measured crack velocities and measured strain distribution on a specified boundary in a specimen or an assumed loading condition during crack propagation as the input condition to drive the crack and then compute energy variations and dynamic fracture toughness through a finite-difference technique based on dynamic elasticity.

Dynamic-fracture-mechanics Analysis of Brittle-crack Propagation and Arrest Test using Ship-hull Steels

Standard-size Double-tension Test

MATERIAL USED IN EXPERIMENT—A 15-mm-thick ship-hull steel (NK code KAS) is used in three types of test specimen. The mechanical properties and chemical compositions of the steel are shown in Table 1.

TESTING PROCEDURE—Two series of standard size double-tension tests are carried out, i.e., a constant-temperature type (SP series) and gradient-temperature type (SA series). In the SP series, a fast crack runs completely through the specimen width. In the SA series, on the other hand, a fast crack decelerates and is arrested because of an increase of material toughness due to temperature gradient. Figure 1 shows the specimen configuration and arrangement of crack-detector gages and strain gages. The specimen consists of a crack-initiation part and a 500-mm-wide crack-propagation part. The specimen is welded to two 30-mm-thick pulling plates, and the total length between two loading pins is about 3000 mm. The welding residual stresses are mechanically relieved by preloading. Uniform tensile stress is applied to the propagation part and a brittle crack is initiated from the super-cooled initiation part by a subload and is run into the propagation part.

T. Kanazawa, S. Machida, T. Teramoto and H. Yoshinari are associated with the Department of Naval Architecture, Faculty of Engineering, University of Tokyo, 3-1 Hongo 7-Chome, Bunkyo-Ku, Tokyo, 113, Japan.

Paper was presented at Fourth SESA International Congress on Experimental Mechanics held in Boston, MA on May 25-30, 1980.

Final manuscript received: August 5, 1980.

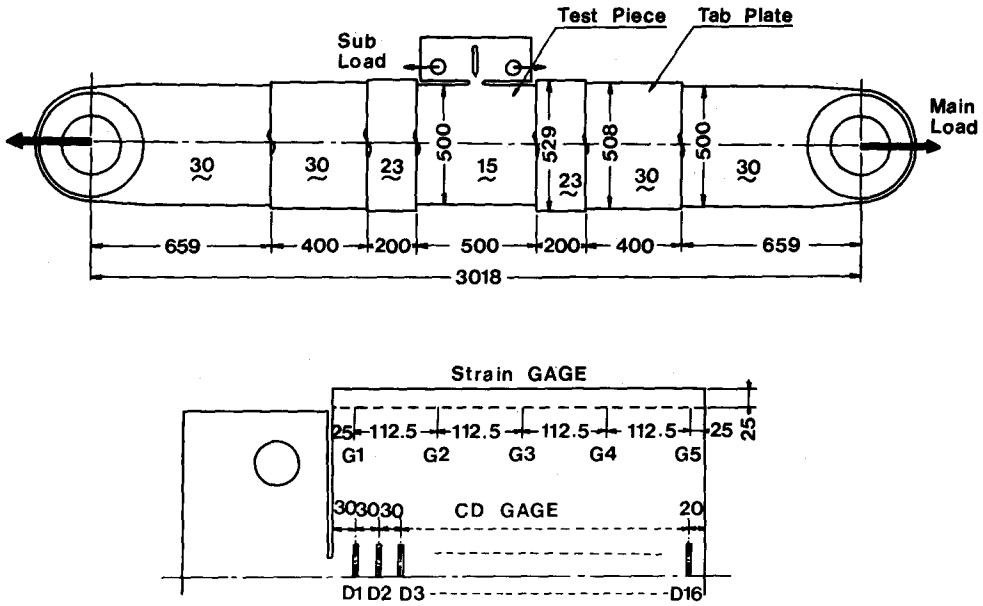

Fig. 1—Specimen configuration and arrangement of crack-detector gages and strain gages

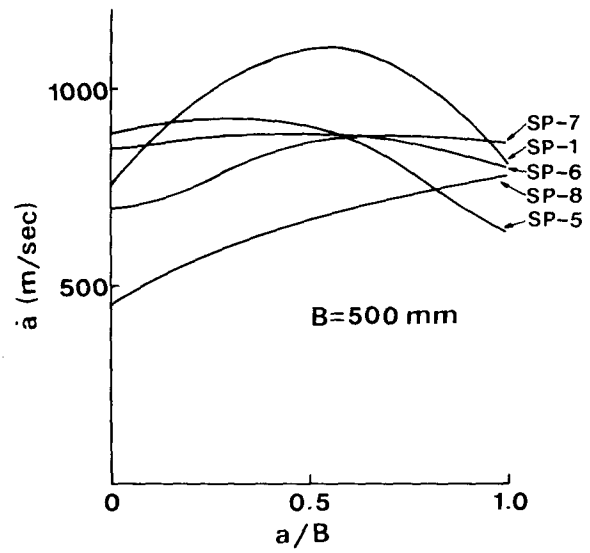

Fig. 2—Variations of crack velocity in SP series test with crack extension

Crack velocity was estimated from crack-tip position vs. time relation detected by progressive cutting of fine wires placed at 30-mm intervals on the propagation part. In the double-tension tests, transient variations of strain distribution with crack extension were measured by five strain gages (designated by G1 to G5 in Fig. 1) placed on the line 225 mm apart from the assumed crack-propagation line.

EXPERIMENTAL RESULTS OF SP AND SA SERIES—The experimental conditions and mean velocities of SP series obtained are shown in Table 2. Four different applied stresses (12, 16, 20 and 24 kg/mm²) were adopted to examine the influence of initial applied stress σ_0 on crack velocity. Testing temperatures are −60°C and −40°C. Figure 2 shows the variation of crack velocity. The crack seems to run at almost constant velocity during crack propagation.

For the SA series using a Type I temperature distribution shown in Fig. 3, four different applied stresses

TABLE 1—MECHANICAL PROPERTIES AND CHEMICAL COMPOSITIONS OF KAS

Mechanical Properties of KAS					
Young's Modulus, E(kg/mm²)	Density, ρ(g/cm³)	Poisson's Ratio, ν	Yield Strength, σ_Y(kg/mm²)	Tensile Strength, σ_u(kg/mm²)	Elongation (%)
20180	8.0	0.287	28	43	34

Chemical Composition (%)				
C	Si	Mn	P	S
0.11	0.33	0.75	0.022	0.008

TABLE 2—EXPERIMENTAL RESULTS OF SP TEST SERIES

	σ_0 (kg/mm²)	T_A (°C)	P_s (Ton)	$\dot{a}_m$ (m/s)	
SP—1	20	−61	6.5	1100	
SP—2	16	−60	25.2	—	Curve
SP—3	24	−60	8	850	Branch
SP—4	16	−61	22.5	—	No Go
SP—5	24	−40	21	1000	
SP—6	20	−40	19	950	
SP—7	16	−42	23.5	900	
SP—8	12	−40	15	750	

TABLE 3—EXPERIMENTAL RESULTS OF SA TEST SERIES

	σ_0 (kg/mm²)	P_s (Ton)	T_A (°C)	a_A (mm)	$\dot{a}$ (m/s)
SA—1	8	20	—	—	—
SA—2	12	11	0	280	650
SA—3	16	7	8	305	750
SA—4	20	20	12	320	1000
SA—5	16	26	14	373	850
SA—6	16	12.5	4	241	750

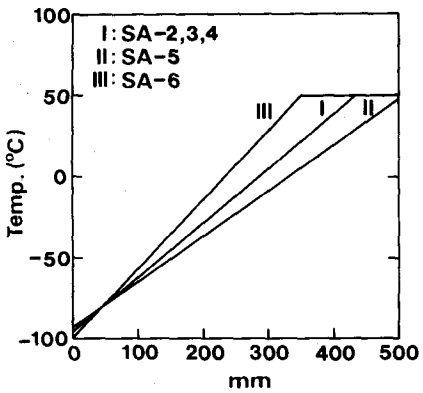

Fig. 3—Temperature distribution for SA series specimen

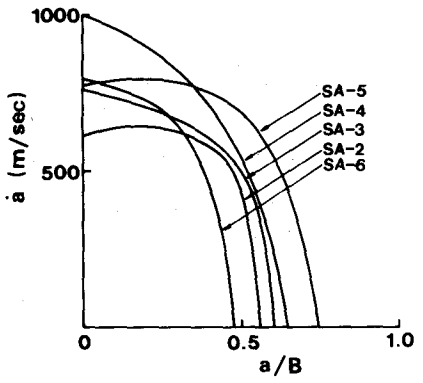

Fig. 4—Variations of crack velocity in SP series test with crack extension

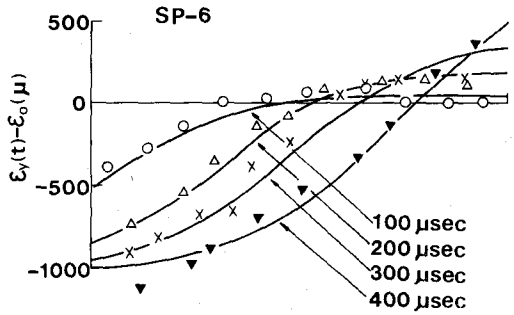

Fig. 5—Comparison between measured and computed variation of strain distribution during crack propagation

(8, 12, 16 and 20 kg/mm²) were adopted. The experiments using Type II and III temperature distributions as shown in Fig. 3, are carried out at σ_0 = 16 kg/mm² to examine the effect of temperature gradient. The experimental conditions and main results are shown in Table 3. T_A and a_A denote temperature at the crack-arrest point and arrested crack length, respectively. Figure 4 shows the variations of crack velocity with crack growth. A crack running rapidly into the propagation part begins to decelerate and is arrested rather abruptly due to the increase of material toughness with temperature.

ANALYSIS AND DISCUSSION—Experimental results are analyzed on the basis of dynamic fracture mechanics from the viewpoint of energetic considerations.

The following equations of motion for a two-dimensional elastic body are numerically solved by the finite-difference method with the experimentally obtained time-dependent boundary conditions.

$$u = C_1^2 u_{,xx} + (C_1^2 - C_2^2) v_{,xy} + C_2^2 u_{,yy}$$
$$v = C_2^2 v_{,xx} + (C_1^2 - C_2^2) u_{,xy} + C_1^2 v_{,yy} \quad (1)$$

where u and v are the displacements in the x and y directions, respectively. The dilatational wave velocity C_1 and distortional wave velocity C_2 are about 5670 m/s and 3100 m/s, respectively. Figure 5 shows an example of the comparison between measured and computed (with the assumption of fixed-grip condition) variation of strain distribution during crack propagation. The ordinate indicates the change in strain from its initial value ϵ_0. The numerals in the figure represent the time elapsed after the trigger is started. Although computed strains show small irregular fluctuation, the general trend of computed strain distribution agrees relatively well with those obtained from the experiment.

The results of analyses under fixed grip conditions do not differ from those under fixed-load condition at all as far as available energy rate and strain distribution on the line are concerned. This may be attributed to the fact that the fast crack ran through the specimen or was arrested before the stress wave reflected from specimen outer boundary (loading ends) came to the boundary concerned (strain-measuring line).

Figures 6(a) and (b) show energy changes due to crack extension under a fixed-grip condition in the SP and SA series, respectively. Static strain-energy changes are also shown in these figures for references. U, K and D denote strain energy, kinetic energy and dissipated energy, respectively. The term D can be obtained indirectly from the law of conservation as follows:

$$D = U_0 - U - K \quad (2)$$

where U_0 means the initial strain energy just before crack initiates. It is generally observed that part of the decrease in U with crack extension is transformed into kinetic energy K and dissipated energy D and, thus, both K and D increase. It is natural that the decrease of U in dynamic case is less than those in static case and the difference of U in two cases becomes larger with the increase of crack length, because of the necessity of kinetic energy for the former case. It is impossible to treat with crack propagation and arrest of a large crack on the basis of static approximation for the above reasons.

Next, assuming that the term D in eq (2) is mostly the energy dissipated in the fractured surface layers, dynamic

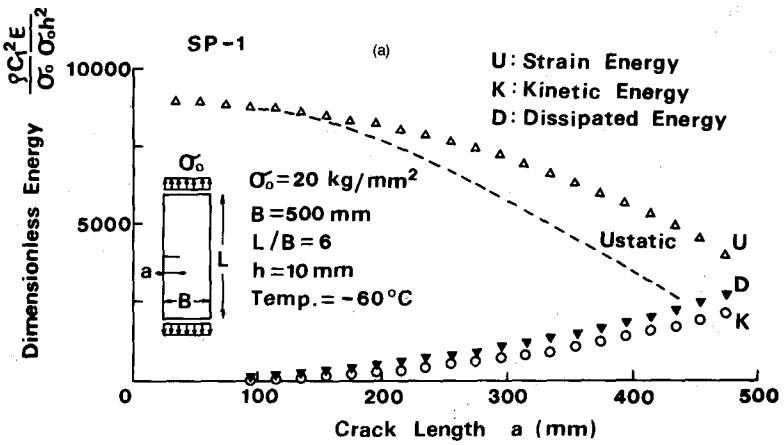

Fig. 6(a), (b)—Energy changes due to crack extension

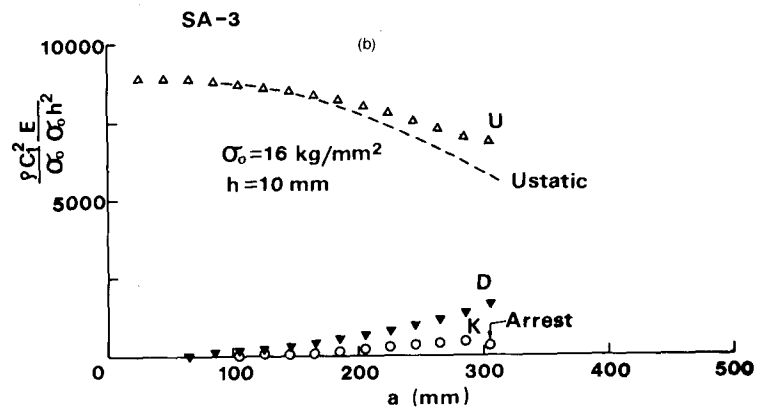

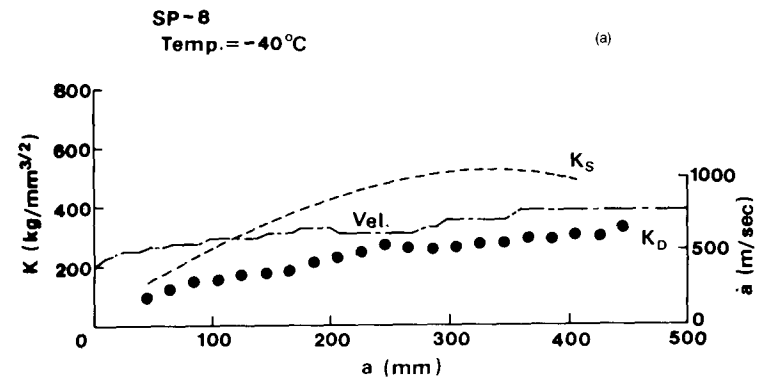

Fig. 7(a), (b)—Variation of dynamic fracture toughness with crack extension

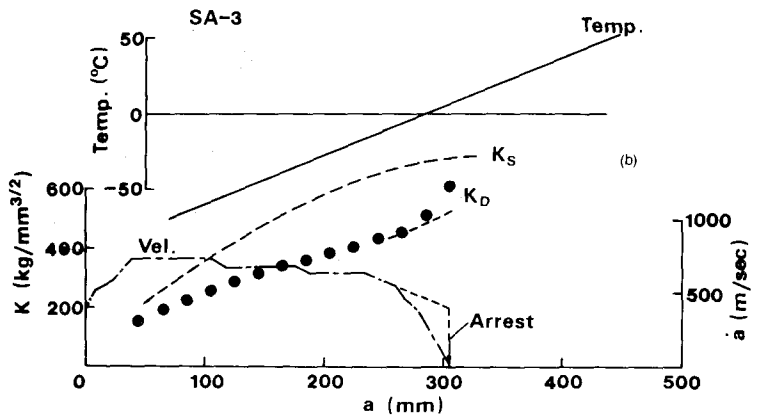

fracture toughness K_D is defined as follows by analogy with the static case:

$$K_D = \sqrt{\frac{E}{1-\nu^2} \cdot \frac{dD}{da}} \tag{3}$$

Figures 7(a) and (b) show the variation of dynamic fracture toughness K_D with crack extension in SP and SA series, respectively. The variation of crack velocity and static stress-intensity factor for the fixed-grip condition are also indicated in each figure for reference. For the SA series, the temperature distribution is also shown in the same figures. In the SP series, a gradual increase of K_D corresponds to the variation of crack velocity. Relatively large increase of K_D with crack extension in the SA series, on the other hand, corresponds not only to the linear increase of temperature, but also its crack-velocity dependence such as observed in SP series. The accuracy of measurement of crack velocity is poor just before crack arrest, because of an extended plastic zone ahead of the crack tip and plate-thickness contraction. Therefore, two types of crack-velocity patterns shown in Fig. 7(b) were used in the analysis. The dashed line in this figure is assumed to account for the existence of lower bound speed. There are some differences of K_D obtained from the above two crack velocities and K_D tends to increase and approach K_s rapidly. This shows the importance of accurate measurement of crack velocity just before the crack is arrested. But the values of K_D are always less than static stress-intensity factor K_s during crack propagation as with the SP series. This is to be noted comparing with the DCB test to be mentioned later.

Large-size Double-tension Test

Wide-plate double-tension tests denoted as SI in this paper have been conducted using the same material at Nagasaki Technical Laboratory of Mitsubishi Heavy Industry Ltd. The results of the two programs where cracks were arrested were subjected to the present analysis. Figure 8 shows the energy changes due to crack extension for the modeled test specimen (1600B × 6000L × 15t mm). Spatial mesh size h is 30 mm. Figure 9 shows the variation of K_D with crack extension. The static stress-intensity factor K_s under fixed-grip condition, the variation of crack velocity and temperature distribution are also shown. The crack velocity is almost constant during crack propagation in these tests and, thus, the increase of K_D is considered to be mainly due to temperature gradient.

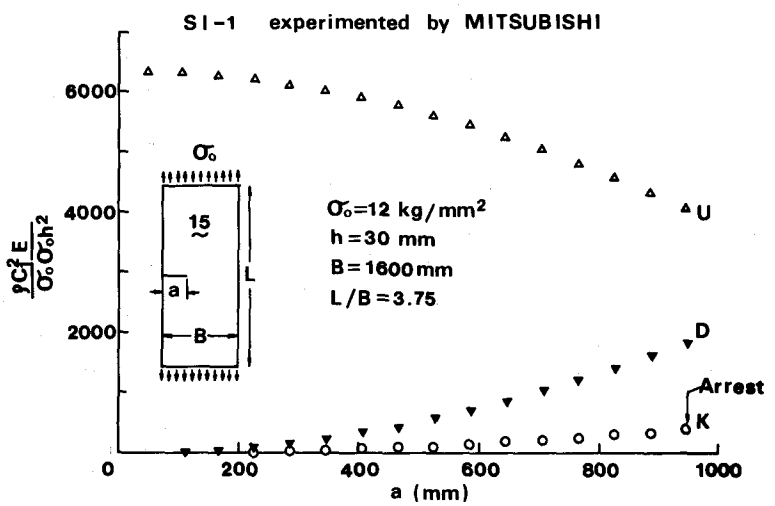

Fig. 8—Energy changes due to crack extension

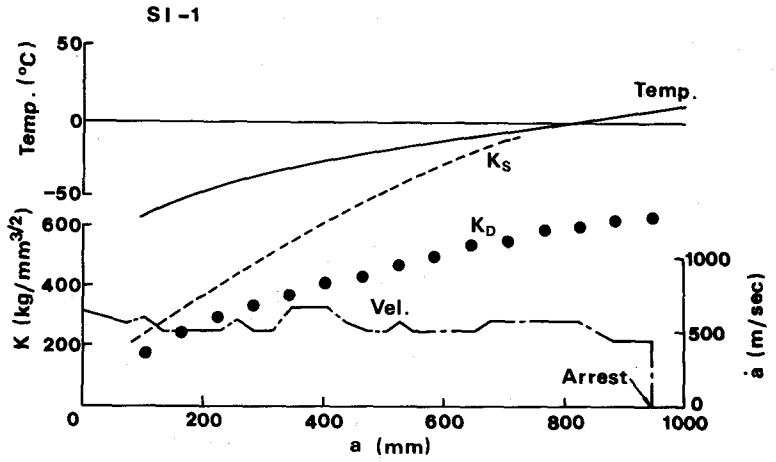

Fig. 9—Variation of dynamic fracture toughness with crack extension

Double-cantilever-beam Test

Experiments using double-cantilever-beam (DCB) specimens made of the same material were carried out and the results were analyzed using a beam-on-elastic-foundation model.[2] The DCB test specimen configuration and the one dimensional model are shown in Fig. 10 and the specimen dimensions are 100(H) × 530(L) × 15(b) (mm).

The specimen is slowly loaded by forcing a split wedge between pins. Since the wedge loading is inherently stiff, crack extension proceeds with essentially constant displacement at the load point. Three experimental results at the temperature of −40°C are analyzed using the finite-difference method as applied to the one-dimensional model.

As an example of calculation results, Figs. 11(a) and (b) show the variation of dynamic material toughness K_D and rates of change in strain and kinetic energies with crack extension. In the case of the double-tension test, K_D is always smaller than K_s and the kinetic energy K increases continuously during crack extension. In this case, during the earlier stage of extension, K_D is smaller than K_s and kinetic energy K increases, but, during the later stage, K_D is larger than K_s and K decreases. It seems that the differences between the DCB test and the double-tension test are caused by the differences of the loading condition and the specimen configuration between the two tests.

The most important result in this section is that, for the DCB specimen, the kinetic energy is almost completely recovered until the crack is arrested. Namely the kinetic energy provides a very significant contribution to maintaining unstable crack extension and dynamic consideration is indispensable.

Dynamic-fracture Characteristics of Ship Steel

The material toughness for fast-crack propagation is to be characterized by putting together the results of three different types of brittle-crack propagation-arrest tests. The material toughness is regarded as governed by two primary parameters, i.e., crack velocity $\dot{a}$ and temperature T, and is expressed by

$$K_D = f(\dot{a}, T) \tag{4}$$

The relation between K_D and crack velocity $\dot{a}$ is obtained from the three types of brittle-crack propagation-arrest test for the temperature of −40°C as shown in Fig. 12. Despite small scatter, it may be concluded that K_D is defined as a specific function of crack velocity for a given temperature, and it is an intrinsic material-characteristic curve independent of specimen configuration and type of loading.

Effect of Specimen Length on the Behavior of Running Cracks

In the previous section, three types of brittle-fracture propagation-arrest tests were conducted and analyzed using the finite-difference technique and it was found that the behavior of brittle-crack propagation and arrest in the double-tension test was quite different from that in

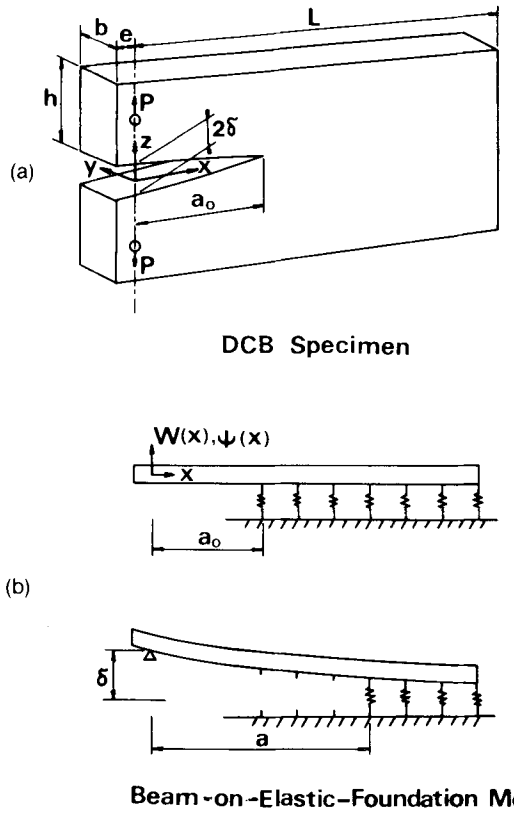

Fig. 10(a), (b)—Configuration of DCB specimen and beam-on-elastic-foundation model

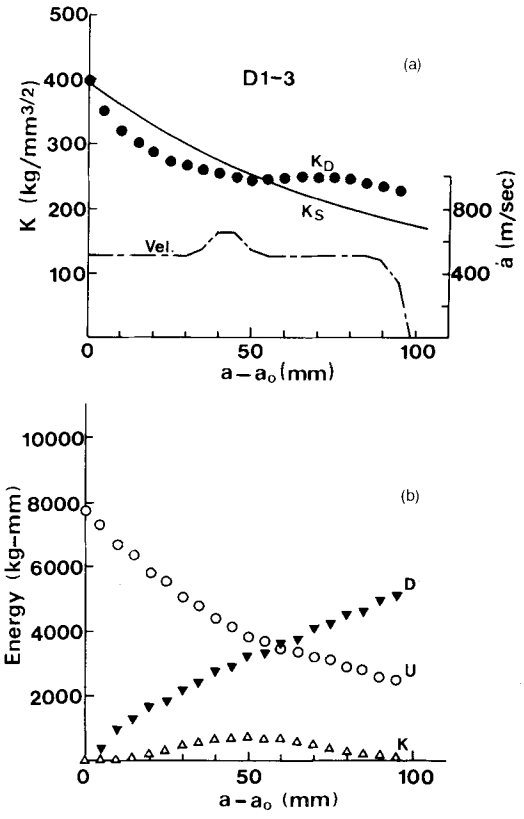

Fig. 11(a), (b)—Variation of dynamic fracture toughness and energies with crack extension in DCB specimen

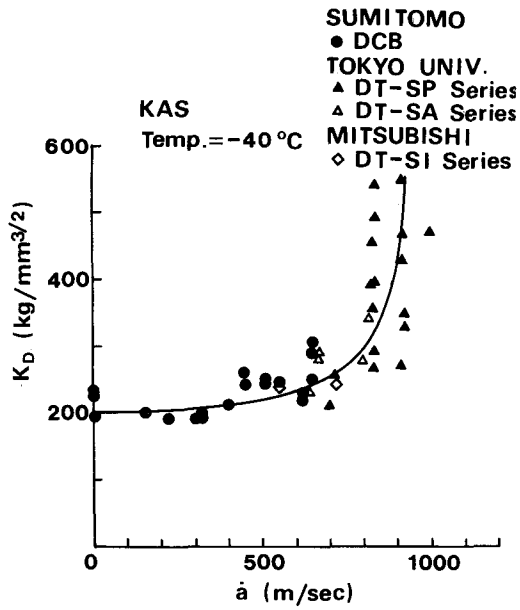

Fig. 12—Dynamic fracture toughness of KAS as a function of crack velocity for the temperature of −40°C

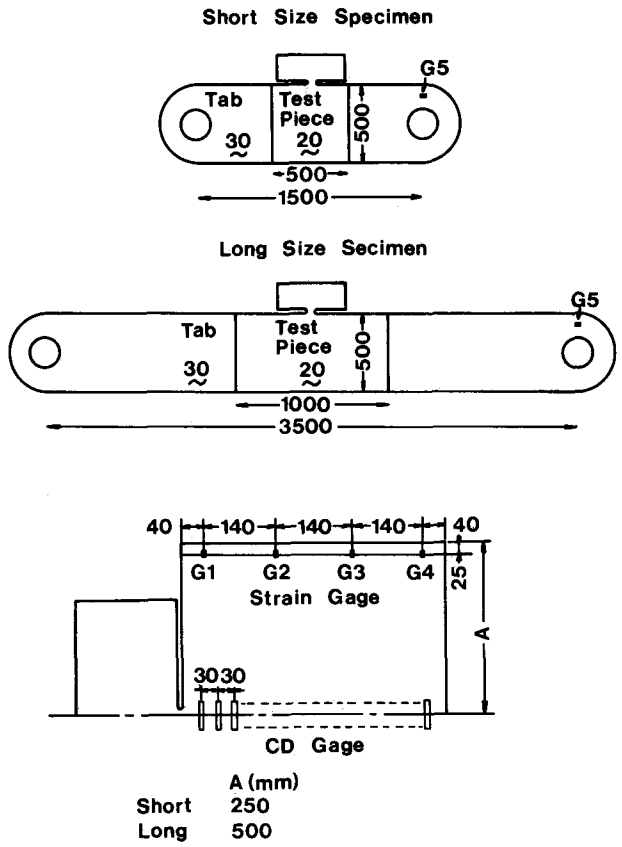

Fig. 13—Specimen configuration and arrangement of crack-detector gages and strain gages

DCB test. Namely, in the DCB test, the kinetic energy initially increased but then decreased and was considerably recovered in a later part of crack propagation and contributed to maintain unstable crack extension, but this was not the case with the double-tension specimen. This is probably because of the large difference in type of loading and the effect of reflected stress waves between these two test methods. This section gives the results of an experimental investigation of the double-tension tests with different lengths between loading ends which were carried out to see how the reflected stress waves from the boundary affects the running crack behavior.

Material Used in Experiment

A 20-mm-thick ship-hull steel (NK code KAS) was used and the mechanical properties and chemical compositions are shown in Table 4.

Test Procedure

The double-tension tests were conducted using two types of temperature distribution in test section, i.e., flat-temperature type for crack-propagation experiment and gradient-temperature type for crack-arrest experiment. Figure 13 shows the configurations for two different distances between the two loading pins and the arrangement of crack-detector gages for crack-velocity measurement and strain gages at the location of G1 to G5 for strain-distribution measurement. The long-size double-tension-test specimen is about 3500 mm long between two loading pins while the short one is about 1500 mm long. The strain variation at G5 is expected to represent the aspect of the variation of load drop. Other testing procedures are same as mentioned in the above section. The following codes will be used to discriminate four different test series:

KLP: long-size test with flat-type temperature
KLA: long-size test with gradient-type temperature
KSP: short-size test with flat-type temperature

TABLE 4—MECHANICAL PROPERTIES AND CHEMICAL COMPOSITIONS OF KAS

Mechanical Properties of KAS

Young's Modulus, E(kg/mm^2)	Density, ρ(g/cm^3)	Poisson's Ratio, ν	Yield Strength, σ_Y(kg/mm^2)	Tensile Strength, σ_u(kg/mm^2)	Elongation (%)
20157	8.0	0.283	28	45	34

Chemical Composition (%)

C	Si	Mn	P	S
0.12	0.23	1.0	0.014	0.009

TABLE 5—EXPERIMENTAL RESULTS OF PROPAGATION TEST

	σ_0(kg/mm^2)	T(°C)	$\dot{a}_m$(m/s)
KLP—1	16	−20	697
KLP—2	16	−10	611
KSP—1	16	−20	632
KSP—2	16	−10	602

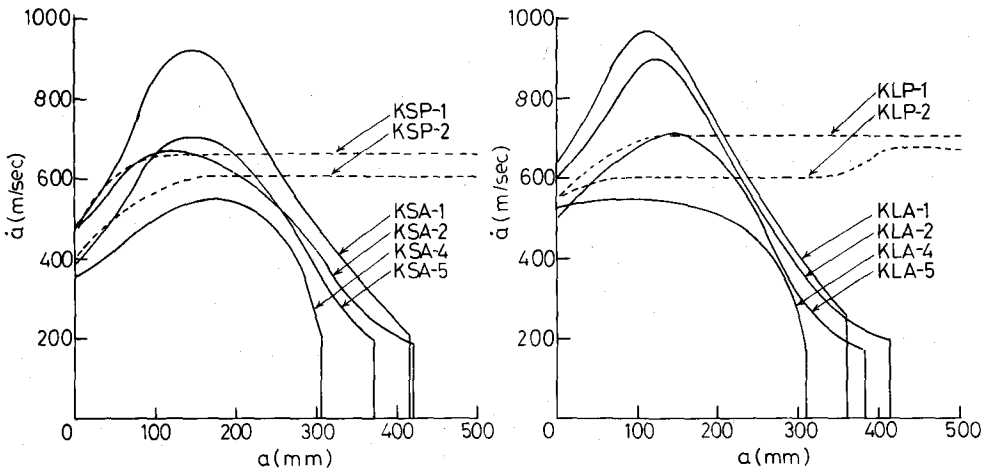

Fig. 14—Variation of crack velocity

KSA: short-size test with gradient-type temperature

Experimental Results

Table 5 shows the experimental results for constant-temperature-type specimens. Initial applied stress is 16 kg/mm² and testing temperatures are −20°C and −10°C. $\dot{a}_m$ denotes attained crack velocity as shown in Fig. 14. The crack velocities in the long-size specimen are a little larger than those in short one. This may be attributed to the fact that, in the long-size series, cracks ran through the whole width of propagation part before the arrival of reflected stress waves from the loading grips, while, in the short-size series, the running crack was affected by the reflected stress waves. In other words, the crack propagation was subjected to a change in loading condition.

Next, the experimental condition and obtained results of gradient-temperature-type (crack-arrest) test series are shown in Table 6. Four different applied stresses (8, 10, 12 and 16 kg/mm²) were adopted to obtain different arrested-crack length a_A and arrest temperature T_A. a_{SL}, $\dot{a}_{SL}$ and T_{SL} in Table 6 represent crack length, velocity and temperature, respectively, at the position where shear lips began to appear as shown in Fig. 15. K_C^A is the apparent arrest toughness on the basis of a static approximation, expressed by

$$K_C^A = \sigma_0 \sqrt{2B \tan\left(\pi a_A / 2B\right)} \qquad (5)$$

where B is the width of propagation part (500 mm). Figure 14 shows the variation of crack velocity with crack extension. As a whole, there is no remarkable difference in crack arrest length and the feature of crack-velocity variation between long- and short-size specimen, but a_{SL} changes systematically between the two series.

TABLE 6—EXPERIMENTAL RESULT OF ARREST TEST

	σ_o (kg/mm²)	a_{SL} (mm)	$\dot{a}_{SL}$ (m/s)	T_{SL} (°C)	a_A (mm)	T_A (°C)	K_C^A (kg/mm$^{3/2}$)
KLA—1	16	323	350	0	363	12	746
KLA—2	12	298	380	−7	412	25.5	712
KLA—4	8	263	390	−16	309	−3	306
KLA—5	10	280	360	−12	379	16.5	500
KSA—1	16	379	330	16	417	27	980
KSA—2	12	360	260	11	423	28.5	764
KSA—4	8	283	350	−11	306	−4	303
KSA—5	10	301	370	−9	371	14	483

Analysis and Discussion

The test results were analyzed by solving eq (1) with the use of the finite-difference technique. Two types of crack-propagation analysis were carried out, i.e., 'whole-field' analysis and 'partial-field' analysis. The former analysis is made on the whole plate including pulling tab plate, as well as test specimen with the loading boundary condition obtained from G5 gage. The latter analysis, on the other hand, is made on a restricted field, i.e., test specimen, using the loading-boundary condition obtained from the measured strain distribution by G1 to G4 gages which varies with crack extension.

Figures 16(a) and (b) show an example of energy changes of long- and short-size specimens due to crack extension by whole analysis. The dissipated energy D is obtained indirectly by W, U and K. A difference of D between long- and short-size specimens is observed beyond crack extension of 300 mm, which seems to be due to effect of length of test specimen, that is, reflected stress waves.

Figures 17(a) and (b) show the variation of dynamic fracture toughness K_D with crack extension (open and solid circles) in the long- and short-size specimens, respectively. In the long-size specimen, K_D tends to increase and approach the approximate static stress-intensity factor expressed by eq (5), especially in the neighborhood of the crack-arresting point.

It was found that, for long specimens, the difference in

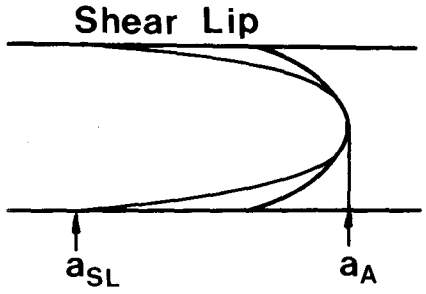

Fig. 15—Fracture-surface appearance near crack tip

boundary condition at loading grip had almost no effect on crack-propagation behavior because the crack propagation was terminated before the stress waves reflected back from the grips reached the running-crack-tip zone. Thus, apparent arrest toughness K_c^A by static approximation is regarded to be valid if test specimen is sufficiently long that there is no effect of reflected stress waves on the running crack tip.

In the short-size specimen, on the other hand, the dynamic fracture toughness K_D is smaller than the tangent form stress-intensity factor during crack propagation although the difference of K_D value between the 'whole' and 'part' analyses also exists. This difference is probably because of inaccuracy of experimentally obtained boundary conditions used as input conditions which has a larger effect through stress-wave reflection for short-size specimens than for longer-size specimens. It is important to know exactly the boundary conditions in order to estimate material toughness, particularly when the specimen size is short. Figure 18 shows the relations between K_D and crack velocity for various temperatures estimated mainly from the results of long-size and short-size crack-arrest test series. The shaded area shows the region where K_D data plots obtained from the propagation series exists. Despite some scatter of data, it is revealed that the dynamic fracture toughness K_D can be expressed as a specific material parameter depending on crack velocity and temperature, namely, Fig. 18 justifies the validity of the expression of eq (4).

Prediction of Fast-crack Propagation

Once the material toughness as expressed by eq (4) is known, the behavior of a fast crack will be predicted by solving the governing equation of motion for the crack expressed by

$$G_d(a,\dot{a}) = G_D(\dot{a},T) = \frac{1-\nu^2}{E} K_D^2(\dot{a},T) \qquad (6)$$

where G_d is crack driving force which depends on crack size, crack velocity, and possibly other geometrical and mechanical boundary conditions, and G_D is the dynamic-fracture-energy rate. But the analytical expression for G_d has been available only for simple limited cases. In general, it is difficult to solve eq (6) without recourse to a numerical technique.

In the following, a preliminary consideration for crack-arrester design will be made with the use of the experimentally obtained K_D for a simple crack.

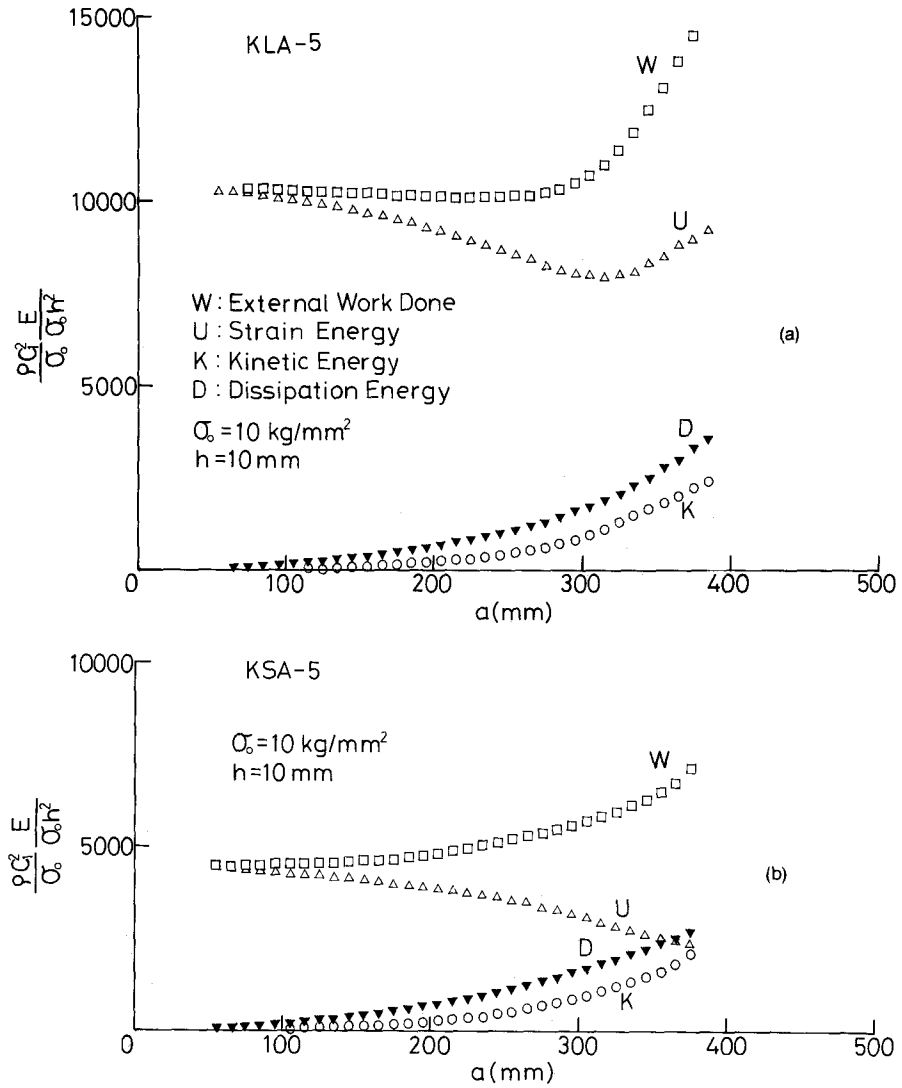

Fig. 16(a), (b)—Energy changes due to crack extension

When a crack propagates in an infinite plate subjected to uniform tensile stress σ, the dynamic stress-intensity factor K_d is given by Freund[3] as

$$K_d(a,\dot{a}) = k(\dot{a})K_s(a) \tag{7}$$

where K_s is the static stress-intensity factor and a universal function of crack speed $k(\dot{a})$ which decreases monotonically with $\dot{a}$ from unity at zero crack speed to zero at the Rayleigh wave velocity C_R. The relation between crack-driving-force rate G_d and dynamic stress-intensity factor K_d is given as

$$G_d(a,\dot{a}) = \frac{1-\nu^2}{E} A(\dot{a})K_d^2(a,\dot{a}) \tag{8}$$

where $A(\dot{a})$ is a monotonically increasing function with $\dot{a}$ and is unity at zero crack speed and becomes unbounded at the Rayleigh wave velocity C_R. From the conservation of energy, the following equation is derived from eqs (6), (7) and (8).

$$k^2(\dot{a})A(\dot{a})K_s^2 = K_D^2(\dot{a},T) \tag{9}$$

As $k^2(\dot{a})A(\dot{a})$ can be approximated by a simple function,[4] eq (9) becomes as follows:

$$K_s \cdot \sqrt{1-\frac{\dot{a}}{C_R}} = K_D(\dot{a},T) \tag{10}$$

The left-hand and right-hand terms of eq (10) correspond to crack driving force and material resistance, respectively. This equation gives crack velocity for given crack length and temperature for a propagating crack in a plate which is so large that the crack never encounters the effect of reflected stress waves from the boundary.

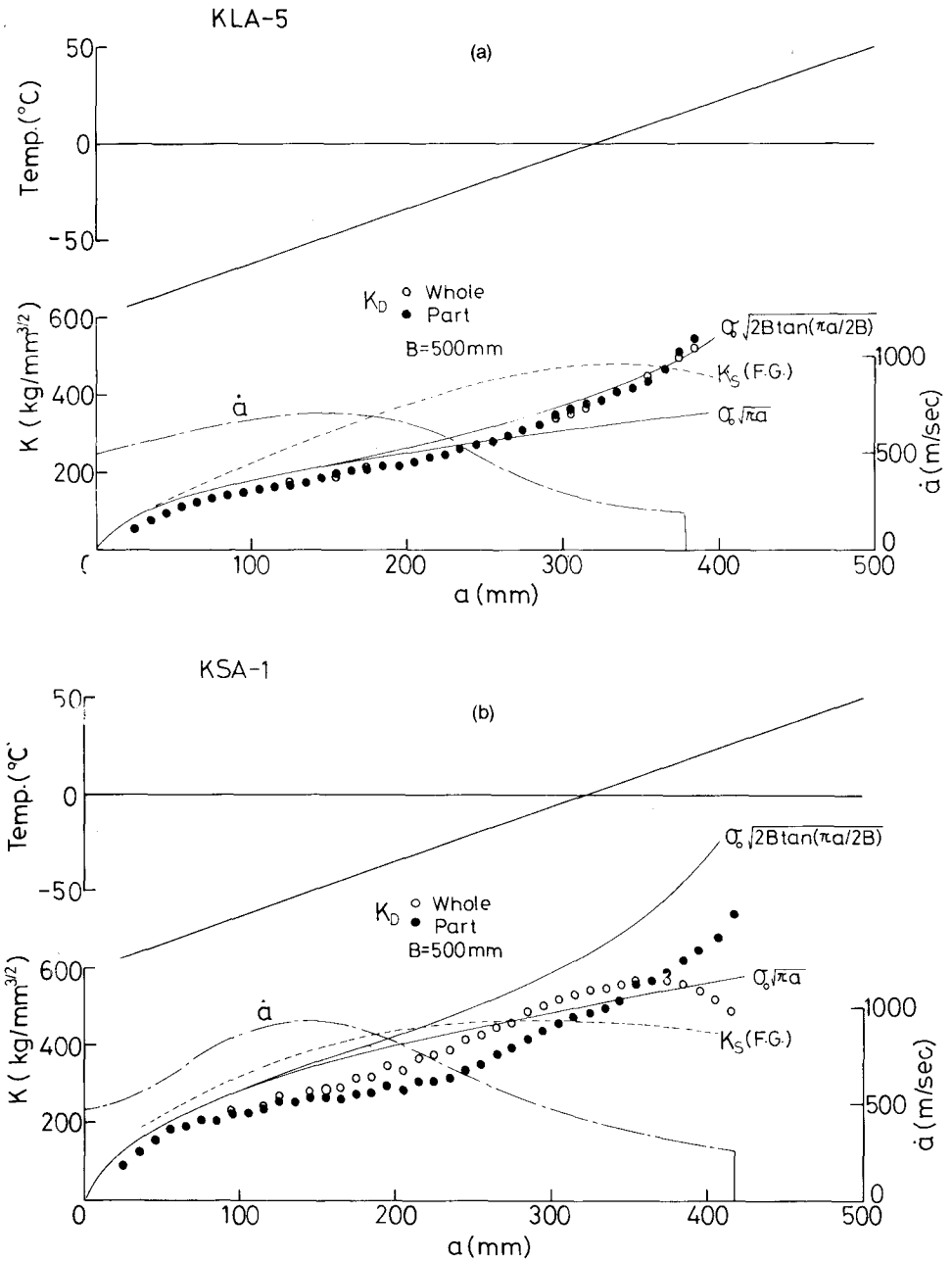

Fig. 17(a), (b)—Variation of dynamic fracture toughness K_D with crack extension

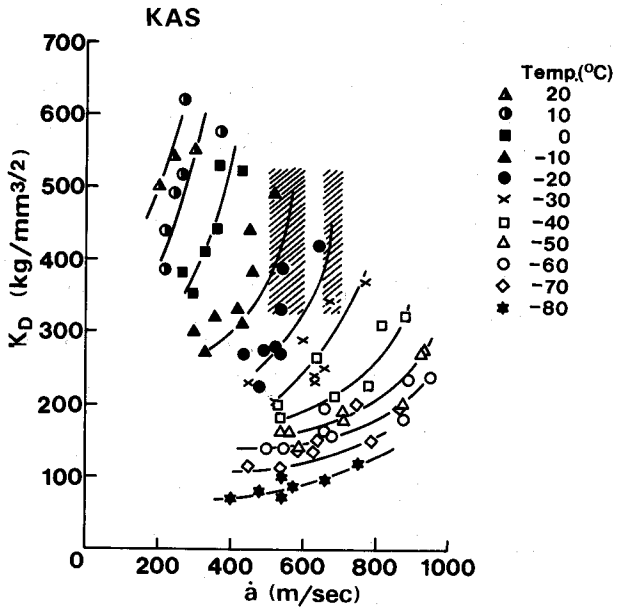

Fig. 18—Dynamic fracture toughness K_D as a function of crack velocity for various temperatures

Figures 19(a) and (b) show the comparison between measured and calculated velocity in a long-size test, which is obtained by solving eq (10) using the toughness curve shown in Fig. 18. K_s is assumed as follows:

$$K_s = \sigma_0 \sqrt{\pi a} \qquad \text{Method I}$$

$$K_s = \sigma_0 \sqrt{2B \tan(\pi a/2B)} \qquad \text{Method II}$$

The calculated crack velocity and crack-arrest length agree well with the experimental values. This is because a crack propagates through the specimen or arrests before an arrival of a reflected stress wave from the boundary to the crack tip. In other words, this specimen may be regarded as an infinite body in this sense.

Therefore, a simple approach will be possible by appropriately defining the amount of contribution of kinetic energy taking due account of the characteristic features of the structural element under consideration. In order to establish an arrest design for a steel structure, it will further be necessary to collect data of clearly defined material toughness and to develop some practical simplification to such an approach which avoids the necessity of complicated dynamic analysis.

Conclusion

The fundamental aspects of brittle-crack propagation and arrest in structural steels have been considered primarily from the energetic point of view for the final goal of establishing a relevant crack-arrester design methodology. Dynamic-fracture-mechanics analysis was made using the finite-difference method on a brittle-fracture propagation-arrest test using a ship steel. Despite the fact that the numerical analysis used is an approximation based on linear theory of elasticity, it is found that dynamic consideration is indispensable for general interpretation of fast fracture and crack arrest and material toughness can be defined as a function of temperature and crack velocity.

Crack-propagation-arrest behavior can be predicted by crack-propagation simulation using the obtained dynamic fracture toughness as expressed in terms of crack velocity and temperature if the condition of loading at the boundary of a specimen (or a structural member) is known. In the case where the effect of reflected stress waves is small, a simple prediction using Freund's formula can be made. This approach is an elementary method of crack-arrester design and more relevant and practical crack-arrester design procedures should be established by taking account of effect of kinetic-energy recovery by a simplified method.

References

1. Kanazawa, T., Machida, S. and Teramoto, T., "Preliminary Approaches to Experimental and Numerical Study on Fast Crack Propagation and Crack Arrest," ASTM STP 627, 39-58 (1977).

2. "Fast Fracture Resistance and Crack Arrest in Structural Steel," SSC-242 Progress Report, Ship Structure Committee (1973).

3. Freund, L.B., "Crack Propagation in an Elastic Solid Subjected to General Loading - I Constant Rate to Extension," J. Mech. Phys. Solids, 20, 129-140 (1972).

4. "A Study of Ship Hull Crack Arrester Systems," Final Technical Report on Project ST-226, Ship Structure Committee (1976).

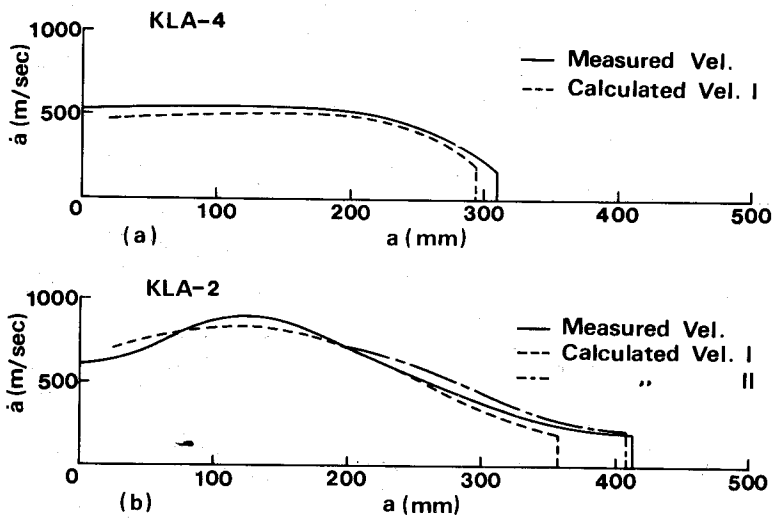

Fig. 19(a), (b)—Comparison between measured and calculated velocity